Recent Results from the BRAHMS Experiment

P. Staszel[a] (for the BRAHMS Collaboration)*

[a]Jagiellonian University, Institute of Physics Institute of Physics,
ul. Reymonta 4, 30-059 Kraków, Poland

We present results obtained by the BRAHMS experiment at the Relativistic Heavy Ion Collider (RHIC) for four colliding systems, namely: Au + Au and Cu + Cu at $\sqrt{s_{NN}} = 200$ GeV and $\sqrt{s_{NN}} = 62.4$ GeV, and d + Au and p + p at $\sqrt{s_{NN}} = 200$ GeV. The focus here is to give an overview of the main results on the reaction dynamics and on the properties of hot and high energy density matter produced in utra-relativistic heavy ion collisions versus its longitudinal expansion. Measurement of particle production, particle spectra over a large rapidity interval as well as high p_T measurements related to nuclear modification in Au + Au and Cu + Cu and d + Au collision are discussed. The observed number of charged particles produced per unit of rapidity at the central rapidity region indicates that a high energy density systems are created at the initial stage of the Au + Au reaction. Analysis of ani-particle to particle ratios (including multi-strange baryon) as the function of rapidity and collision energy reveals that particles population at the chemical freeze-out stage for heavy ion reaction at and above SPS energies is controled only by baryon chemical potential. From the particle spectra we deduced significant radial expansion ($\beta \approx 0.75$) which is consistent with the large initial energy density. We also measured the elliptic flow parameter v_2 versus rapidity and p_T. The weak dependency (if any) of the $v_2(p_T)$ is observed. We present rapidity dependent p/π rations in $0 < y < 3$ for Au + Au and Cu + Cu $\sqrt{s_{NN}} = 200$ GeV. The strong enhancement of proton and anti-proton yields compared to pion yields is seen, and the results are discuss in terms of collision energy, system size and rapidity dependency. We compare R_{AuAu} for Au + Au at $\sqrt{s_{NN}} = 200$ GeV and $\sqrt{s_{NN}} = 62.4$ GeV, and for Au + Au and Cu + Cu at $\sqrt{s_{NN}} = 200$ GeV. The general observed trend is that R_{AuAu} increases with: decreasing collision energy, system size, and collision centrality. R_{AuAu} shows very weak dependency on rapidity (in $0 < y < 3.2$ interval), both for pions and protons.

1. INTRODUCTION

Reactions between heavy nuclei provides a unique opportunity to produce and study nuclear (hadronic) matter far form its ground state, at extremely high densities and temperatures. From the onset of the formulation of the quark model and the first understanding of the nature of the binding and confining potential between quarks about 30 years ago, it has been realized that at very high density and temperature the hadronic

*For the full BRAHMS Collaboration author list and acknowledgment see appendix 'Collaborations' of this volume

matter may undergo transition to the more primordial form of matter characterized by a strongly reduced interaction between its constituents, quarks and gluons, such that the partons would exist in the nearly free state. This proposed state of matter has been designated the quark gluon plasma (QGP).

Experimental attempts to create the QGP in the laboratory by colliding heavy nuclei have been carried out for more than 20 years. During that period, center of mass energies per pair of colliding nucleons have risen steadily from the $\sqrt{s_{NN}} = 1$ GeV domain of the Bevalac at LBNL, to energies of $\sqrt{s_{NN}} = 5$ GeV at the AGS at BNL, and to $\sqrt{s_{NN}} = 17$ GeV at the SPS at CERN. Although a number of signals suggesting the formulation of a very dense state of matter, no strong evidence for QGP formation was found at these energies.

In mid-August 2001 systematic data collecting by the four RHIC experiments, namely BRAHMS, PHENIX, PHOBOS and STAR, began at the energy of $\sqrt{s_{NN}} = 200$ GeV. The RHIC operations started a new era of systematic studies of strongly interacting matter created in ultra-relativistic nucleus-nucleus collision. The main results obtained up to present at RHIC are the large eliptic flow observed for central Au + Au collisions, consistent with the hydrodynamic evolution of the perfect fluid [1–3], and the strong jet suppresion [4] predicted within the Quantun Chromo-Dynamic theory, (QCD), as a consequence of creation of the dense colored medium [5]. The last observation was supplemented by d + Au measuremet showing absence of suppresion, and rather Cronin type enhancent at the central rapidity region that excluded alternative interpretation of suppresion in term of initial state parton saturation (CGC) effects. Another measurement that strongly supported the scenarion of jet quenching was the discovery of mono-jet production [6,7] in central Au + Au collisions, whereas, for d + Au and pheripheral Au + Au near side and away side back-to-back jet correlation have been measured. The large rapidity range and p_T coverage allows BRAHMS to study the properties of the produced medium as a function its longitudinal expansion. The measurement of the evolution of R_{dAu} on rapidity performed by BRAHMS shown that at more forward rapidities the hadronic yields are suppresed as compare to scaled p + p interactions [8]. The suppresion was even stronger for central collitions. Both observetions can be quantitatively describeed within the framework of CGC [5,9].

2. BRAHMS DETECTOR SETUP

The BRAHMS (Broad RAnge Hadron Magnetic Spectrometers) [10], experimental setup consists of global detectors, and two spectorometer arms: Mid-Rapidity Spectrometer (MRS) that operates in the polar angle range from 30-90 degree, and the Forwad Spectrometer (FS) that operates in the range between 2 and 20 degree. Global detectors can measure the global features of the collision like overall particle multiplicity and centrality, collision vertex position, and right now they provide also reaction plane orientation for the azimuthal flow analysis. For the momentum measurements in the MRS we use two tracking devices and one dipol magnets. Particle identification (PID) is done by the Time of Flight (TOF) measurements and K/p separation is extended by using cherenkov detector C4. In the FS two Time Projection Chambers (TPC) and three Drift Chambers (DC) deliver particle track segments and for the momentum measurement we

use three dipol magnets. The PID is provided by TOF measurements for low (TOF1) and medium (TOF2) particle momenta, and by Ring Imaginary Cherenkov detector (RICH) in the high momentum mode measurement. The BRAHMS PID ability is summarized in Table 1. Using 2 σ cut, in MRS we have K/π separation up to 2.5 GeV and K/p

Table 1
Upper range of the momentum for 2σ separation (in GeV/c)

	$0 < \eta < 1.0$			$1.5 < \eta < 4.0$		
	TOFW	TOFW2	C4	TOF1	TOF2	RICH
K/π	2.0	2.5	-	3.0	4.5	25.0
K/p	3.5	4.0	9.0	5.5	7.5	35.0

separation up to 4 GeV, C4 allows to extend the K/π separation up to 9 GeV. In the FS, the TOF measurement provide separation up to 4.5 GeV for K/π and up to 7.5 GeV for K/p. RICH extends this ability up to 25 GeV for K/π and provides proton id up to 35 GeV.

3. OVERALL BULK CHARACTERISTICS

The multiplicity distribution of emitted particles is a fundamental observable in ultra-relativistic collisions. It is sensitive to all stages of the reaction and can address issues like the role of hard scatterings between partons and the interaction of these partons in the high-density medium [11–13]. Figure 1 shows the measured pseudo-rapidity density of charged hadrons, $\mathrm{dN}_{ch}/\mathrm{d}\eta$, over a wide range of η for different centralities indicated on the plot. For the most central collisions $(0-5\%)$ we observed about 4500 of charged particles within the rapidity range covered and the $\mathrm{dN}_{ch}/\mathrm{d}\eta\,|_{\eta=0} = 625 \pm 56$. The last value exceeds the particle production per participant pair observed in elementary p + $\bar{p}$ collisions at the same energy by 40-50% [14]. This means that nucleus-nucleus collisions at the considered energies are far from being the simple superposition of elementary collisions.

This simple measurement of charged particle density $dN_{ch}/d\eta$ can be used to estimate the so called Bjorken energy density, ε [15]. The formula

$$\varepsilon = \frac{3}{2} \times \frac{\langle E_t \rangle}{\pi R^2 \tau_o} \times \frac{dN_{ch}}{d\eta} \tag{1}$$

provides the value of $\approx$ 4 GeV/fm^3. In (1) we assumed that τ_o = 1 fm/c, $\langle E_t \rangle$ = 0.5 GeV and R = 6 fm. The factor 3/2 is due to the assumption that the charged particles carried out of the reaction zone only a fraction (2/3) of the total available energy. The more refined results obtained from the identified particle spectra calls for larger value of 5 GeV/fm^3 ($\sqrt{s_{NN}}$ = 200 GeV), 4 GeV/fm^3 ($\sqrt{s_{NN}}$ = 130 GeV), and 4 GeV/fm^3 ($\sqrt{s_{NN}}$ = 130 GeV), [16]. All these values significantly exceed the predicted energy density for the boundary between hadronic and partonic phases [17]. For $\sqrt{s_{NN}}$ = 200 GeV the energy density exceeds by factor of 30 the density of normal nuclear matter and by a factor of 5 the density of a single baryon.

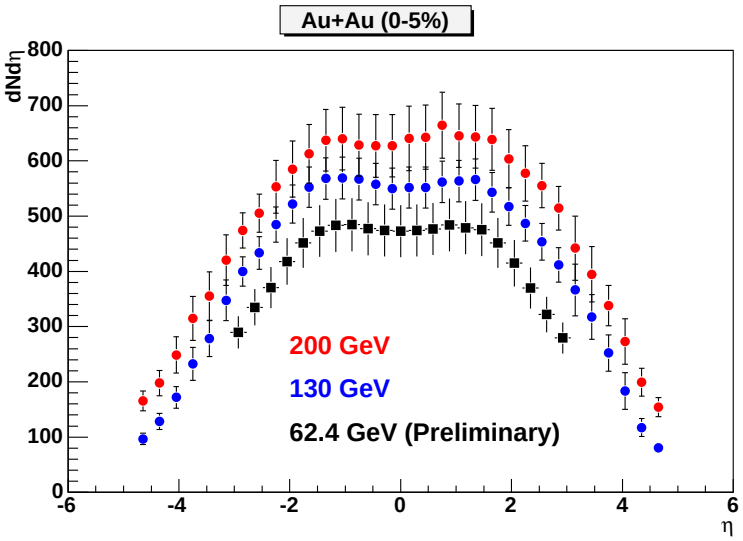

Figure 1. Distributions of $dN_{ch}/d\eta$ measured by BRAHMS for $0-5\%$ central Au + Au reactions, at $\sqrt{s_{NN}} = 200$ GeV, $\sqrt{s_{NN}} = 130$ GeV and $\sqrt{s_{NN}} = 62.4$ GeV *(Waiting for improved plot from Steve).*

3.1. Chemistry with BRAHMS

BRAHMS measured also the anti-particle to particle ratios for pions ($N(\pi^-)/N(\pi^+)$), kaons ($N(K^-)/N(K^+)$) and protons ($N(\bar{\mathrm{p}})/N(\mathrm{p})$) over the large rapidity interval. The results, for Au + Au collision at $\sqrt{s_{NN}} = 62.4$ GeV and $\sqrt{s_{NN}} = 200$ GeV are presented on Figure 2. Whereas $N(\pi^-)/N(\pi^+)$ stays constant and is equal 1 in the whole covered rapidity range ($0 < \mathrm{y} < 3.2$) for the all RHIC energies the $N(K^-)/N(K^+)$ and $N(\bar{\mathrm{p}})/N(\mathrm{p})$ drop significantly with increasing rapidity. For ($\sqrt{s_{NN}} = 200$ GeV) the $N(K^-)/N(K^+)$ and $N(\bar{\mathrm{p}})/N(\mathrm{p})$ equal respectively 0.95 and 0.76 at $y \approx 0$ reach values of 0.6 for $N(K^-)/N(K^+)$ and 0.3 for $N(\bar{\mathrm{p}})/N(\mathrm{p})$ around rapidity 3. Comparing $\sqrt{s_{NN}} = 200$ GeV and $\sqrt{s_{NN}} = 62.4$ GeV we observe 11% and 40% decrease of rations at mid-rapidity and 43% and 93% decrease at $y \approx 3$ for kaons and protons, respectively. The large difference in the $N(\bar{\mathrm{p}})/N(\mathrm{p})$ reduction for $y \approx 0$ and $y \approx 3$ is due to the fact that for the lower energy the vicinity of $y \approx 3$ corresponds to the fragmentation region, whereas for $\sqrt{s_{NN}} = 200$ GeV $y = 3$ lies about 1 unit of rapidity below the maximum in the net-baryon distribution [18].

Figure 3 shows the $N(K^-)/N(K^+)$ as a function of corresponding $N(\bar{\mathrm{p}})/N(\mathrm{p})$ for various rapidities. The data are for central collisions for the three studied incident energy. AGS and SPS results are plotted for comparison. There is a striking correlation between the RHIC/BRAHMS kaon and proton ratios over 3 units of rapidity. It is worth to note that the BRAHMS forward rapidity data measured at $\sqrt{s_{NN}} = 62.4$ GeV overlap with the SPS points that were measured at much lower energy but at mid-rapidity. The solid line plotted on the figure refers to the fit with a statistical model assuming that the temperature at the chemical freeze-out is 170 MeV [19,20]. It is seen that the data are well described by the statistical model over the broad rapidity range with baryonic chemical potential changing from 27 MeV at mid-rapidity to 140 MeV at the most forward ra-

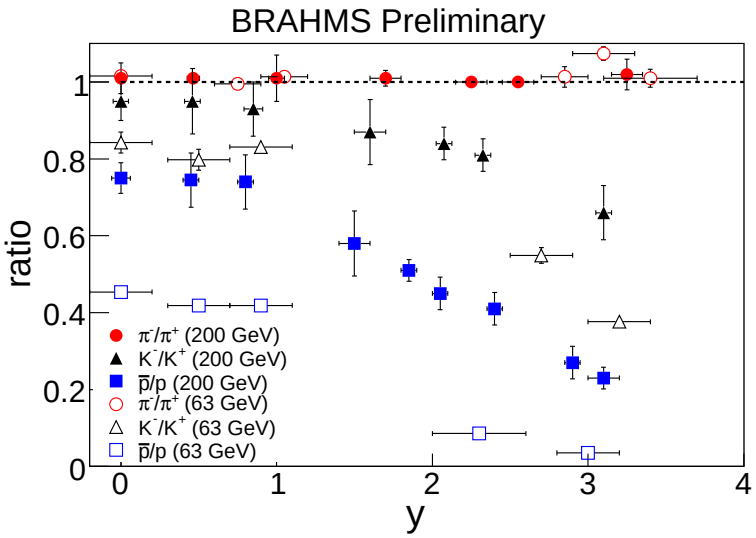

Figure 2. Ratios of anti-particles to particles (pions, kaons and protons) at a function of rapidity for $\sqrt{s_{NN}} = 62.4$ GeV, $\sqrt{s_{NN}} = 200$ GeV. Statistical and systematic errors are indicated.

pidities. Assuming that we can use statistical arguments based on chemical and thermal equilibrium at the quark level, the ratios can be written

$$\frac{N(\bar{p})}{N(p)} = e^{-6\mu_{u,d}/T}, \qquad \frac{N(K^-)}{N(K^+)} = e^{-2(\mu_{u,d}-\mu_s)/T}, \tag{2}$$

where μ and T are chemical potential and temperature, respectively. Assuming that $\mu_s = 0$, from (2), one gets $N(K^-)/N(K^+) = [N(\bar{p})/N(p)]^{1/3}$. This relation, represented by dotted line on Figure 3, does not reproduce the observed correlation. The data are however well fitted by the function $N(K^-)/N(K^+) = [N(\bar{p})/N(p)]^{1/4}$ (dashed line) which is consistent with (2) assuming $\mu_s = 1/4\mu_{u,d}$.

Recently, STAR and NA49 have measured mid-rapidity $\bar{\Lambda}/\Lambda$, $\bar{\Xi}/\Xi$ and $\bar{\Omega}/\Omega$ versus $\bar{p}$ to p rations for set of energies from $\sqrt{s_{NN}} = 10$ GeV up to $\sqrt{s_{NN}} = 200$ GeV. These measurements of strange and multi-strange particles ratios provide the possibility to test the relation between μ_s and $\mu_{u,d}$ found for kaons. From the model of chemical and thermal equilibrium at the quark level one can derive the following relations

$$\frac{N(\bar{H})}{N(H)} = \left[\frac{N(\bar{p})}{N(p)}\right]^A, \tag{3}$$

where H stands for any hadronic states build of u, d and/or s quarks. Taking $\mu_s = 1/4\mu_{u,d}$, one can easily calculate that the A is equal 3/4 for Λ, 1/2 for Ξ and 1/4 for Ω. The predicted $\bar{\Lambda}/\Lambda$, $\bar{\Xi}/\Xi$ and $\bar{\Omega}/\Omega$ versus $\bar{p}/p$ functions are plotted on Fig. 4, and the data points are for NA49 (open symbols) and STAR (solid symbols) measurements of strange ani-particle-to-particle rations measured at mid-rapidity. (The parameters A extracted from fits are equal 0.74 ± 0.02, 0.55 ± 0.02 and 0.21 ± 0.08 for Λ, Ξ and Ω, respectively.) The agreement predictions based on K^-/K^+ ratios measure at different rapidities with antihyperons-to-hyperons rations measured at mid-rapidity is noticeable, and the established relation $\mu_s = 1/4\mu_{u,d}$ calls for the theoretical explanation.

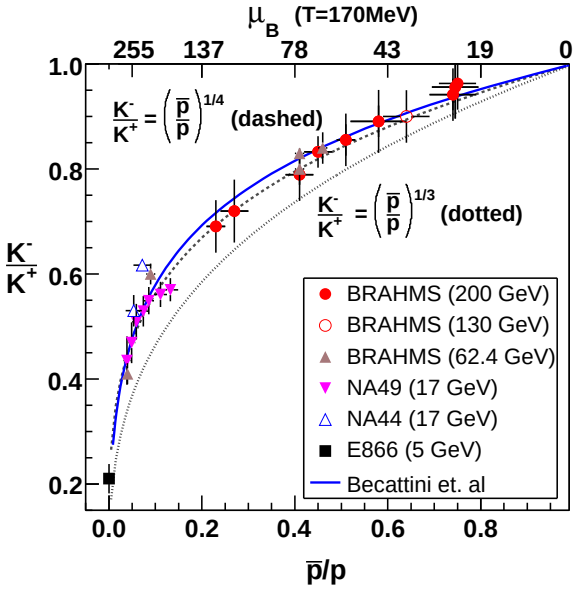

Figure 3. Correlation between $N(K^-)/N(K^+)$ and $N(\bar{p})/N(p)$. The solid curve refer to statistical model calculation with a chemical freeze-out temperature of 170 MeV

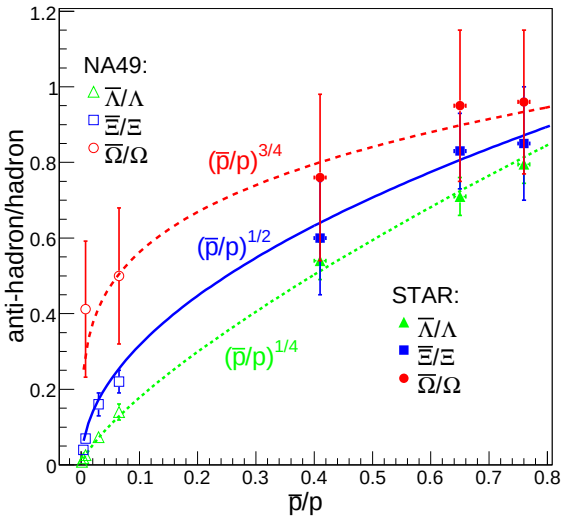

Figure 4. Anti-particle to particle ratios for Λs, Ξs and Ωs as a function of $\bar{p}/p$. Different points show mid-rapidity ratios measured by NA49 and STAR collaboration at different collision energies. Meaning of the plotted functions is explained in text

3.2. Radial flow

The properties of matter in the latest stage of the collision when the interactions between particles cease (kinetic freeze-out) can be studied from the shape of spectra of the emitted particles. This shape depends in general on the temperature of the emitting source and on the collective flow. For central collisions where one should not expect any azimuthal dependency only so called transverse (radial) flow is important [3]. In the so-called blast-wave approach the spectrum is parametrized by a function depending on the freeze-out temperature, (T_{fo}), and on the transverse expansion velocity (β_T). Figure 5 shows results from analysis of the particle spectra from the Au + Au reaction at $\sqrt{s_{NN}}$ = 200 GeV using the blast-wave model fit, simultaneously to π^+, π^-, K^+,K^-, protons and anti-protons, plotted versus number of participants (N_{part}).

The obtained result indicates that the kinetic freeze-out temperature decreases with centrality from about 140 MeV for $40-50\%$ centrality bin to about 120 the most central collisions. The second quantity is lower than the temperature of the chemical freeze-out indicating that, as expected, the freeze-out of particle ratios occurs earlier than the kinetic freeze-out. The reversed trend is seen for the expansion velocity which is equal about 0.65c and 0.75c for $40-50\%$ centrality and $0-5\%$ centrality class, respectively. For comparison we shown also the results for Cu + Cu colliding at the same energy. For the same N_{part} value the T_{fo} for both systems is very similar, however, the reduction of

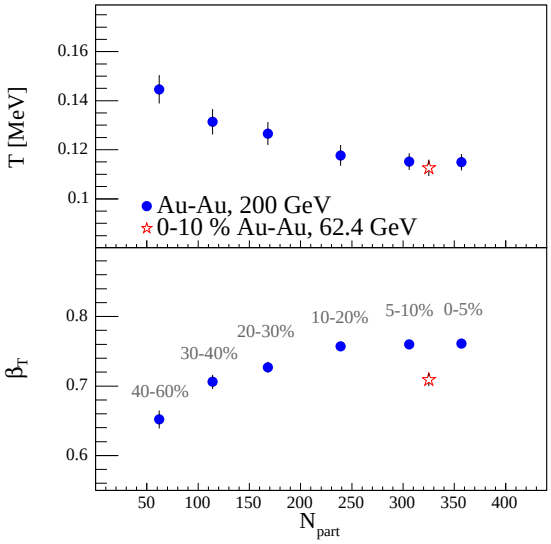

Figure 5. Kinetic freeze-out temperature and transverse flow velocity at mid-rapidity as a function of centrality for Au + Au and Cu + Cu collisions at $\sqrt{s_{NN}} = 200$ GeV.

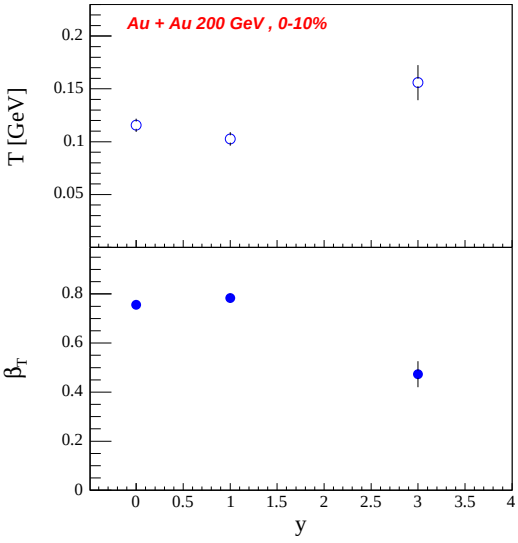

Figure 6. Kinetic freeze-out temperature and transverse flow velocity for central Au + Au at $\sqrt{s_{NN}} = 200$ GeV as a function of rapidity.

about 20% in expansion velocity is observed.

The similar anti-correlation between T_{fo} and β_T is observed for the rapidity dependence, see Figure 6. The trends are consistent with the hydrodynamic description in which the radial flow is the result of outwards gradients of pressure which exists in the expanding matter during the whole evolution. Thus the speed of expansion should increase with the density of the initially created system. The transverse flow velocity is larger than that observed at SPS energies. This is consistent with a large initial density of the system created at RHIC.

3.3. Elliptic Flow

The powerful tool to study the dynamic that drown the evolution of systems created in heavy ion reactions is the analysis of the azimuthal distribution of the emitted particles relative to the reaction plane. The triple differential distribution of emitted particles can be factorized as follow

$$\frac{dN}{dydp_Td\phi} = \frac{dN}{dydp_T}\frac{1}{2\pi} \times (1 + 2v_1(y, p_T)cos\phi + 2v_2(y, p_T)cos2\phi + ...). \quad (4)$$

where ϕ and ϕ_r denote the azimuthal angles of the particle and of the reaction plane, respectively. The first factor depends only on y and p_T and the second factor represents the expansion of the azimuthal dependence into the Fourier series. The coefficients at the first (v_1) and the second (v_2) harmonics, are called direct and elliptic flow parameter, respectively, and in principal they are function of rapidity and transverse momentum. The calculations based of hydrodynamical models [3] show that the elliptic flow can be

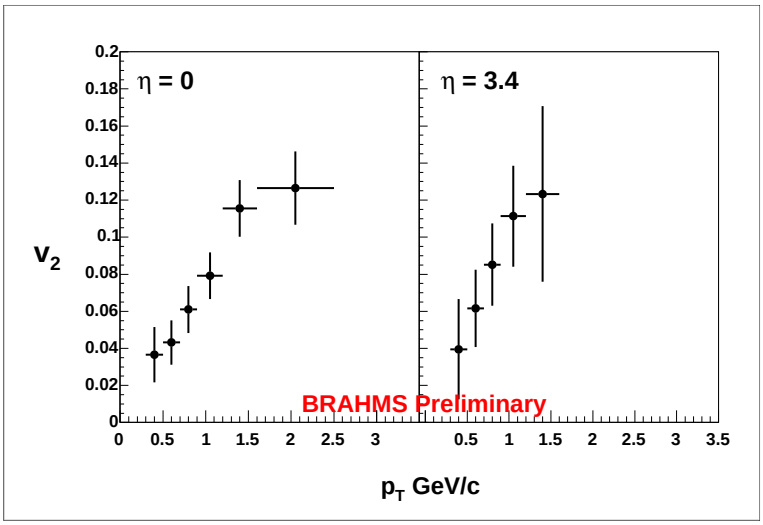

Figure 7. Pion elliptic flow parameter p_T dependence measured for Au + Au at $\sqrt{s_{NN}}$ = 200 GeV at $\eta = 0$ and at $\eta = 3.2$.

generated mainly during the highest density phase, before the initial spatial anisotropy of created medium disappears. Thus v_2 is sensitive only to the very early phase in the system evolution and relatively insensitive to the late stage characterized by the dissipative expansion of the hadronic gas.

BRAHMS has measured the p_T dependence of v_2 at central and forward rapidity, The results are shown on Figure 7. The reaction plane was determined for each event by using the array of azimuthally arranged silicon and tails detectors (see [21]). At mid-rapidity the emitted hadrons have been measured in MRS and at forward rapidities by FS. The BRAHMS results at $\eta \approx 0$ are consistent with the same measurements by STAR collaboration [6]. Figure 7 shows the striking weak (or lack) of $v_2(p_T)$ rapidity dependence. (should refer to Hiro for more conclusions).

4. BARYON TO MESON RATIOS

With its excellent particle identification capacities BRAHMS can study the the p_T and rapidity production dependency for different type of hadrons. Preliminary results [22,23] indicate that for Au + Au reactions in the intermediate p_T region the proton to meson ratio is significantly higher that one would expected from the parton fragmentation in vacuum. Several theoretical explanation in terms of partonic interaction have been proposed like models of quark hadronization and quark coalescence [24–26] and models that incorporate the novel baryon dynamics [**?**]. The recent experimental data obtained for the p + p, Au + Au, and Cu + Cu colliding systems are expected to result in a better understanding of the underlying physics and verification of the proposed theoretical scenarios. Fig. 8 shows a recent investigation by BRAHMS ([27]) of the $\bar{p}$ to π^- ratios at mid-rapidity (circles) and at pseudo rapidity $\eta = 3.2$ (squares) for different Au + Au collisions at $\sqrt{s_{NN}} = 200$ GeV centrality classes indicated on the plot. The bottom panel shows the ratios for p + p at $\sqrt{s_{NN}}$ = 200 GeV measured by PHENIX at mid-rapidity and by BRAHMS at forward rapidity. The data reveal the smooth increase of $\bar{p}/\pi^-$ from peripheral to

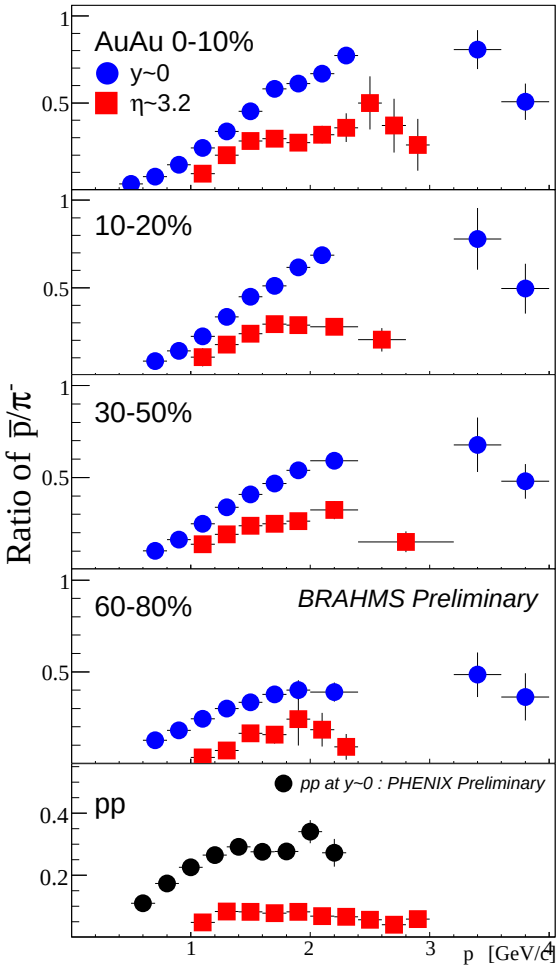

Figure 8. The $\bar{p}$ to π^- ratios at mid-rapidity (circles) and at pseudo rapidity $\eta = 3.2$ (squares) for different Au + Au and p + p collisions at $\sqrt{s_{NN}} = 200$ GeV.

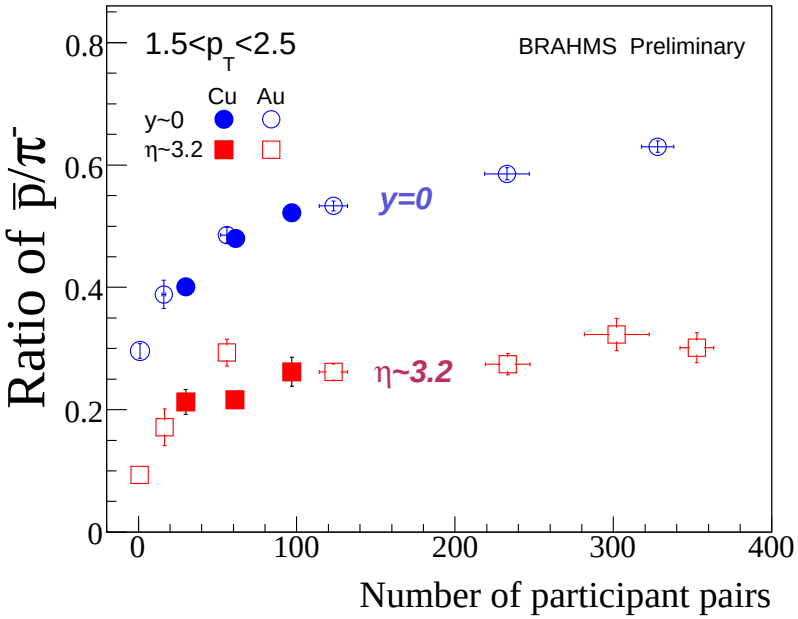

Figure 9. The $\bar{p}/\pi^-$ versus N_part for Au + Au (open symbols) and Cu + Cu (solid symbols) at $\sqrt{s_{NN}} = 200$ GeV.

central collisions, the centrality dependence is however stronger at mid-rapidity than at forward rapidity. The rations increase with increasing p_T in the p_T range up to about 3 GeV/c and 2 GeV/c for mid and forward rapidity, respectively, and above these values the ratios start to decrease. Figure 9 presents the $\bar{p}/\pi^-$ centrality dependence for Au + Au (open symbols) and Cu + Cu (solid symbols) at $\sqrt{s_{NN}} = 200$ GeV. The data for $y = 0$ and $\eta = 3.2$ are represented by circles and squares, respectively. It is seen the strong increase $\bar{p}/\pi^-$ in the N_{part} range from 0 to 100. Above 100 the dependency on the N_{part} is much weaker and the rations reach value of about 0.6 and about 0.25 for mid and forward rapidity, respectively. It is important to note that the Au + Au and Cu + Cu ratios are consistent with each other when plotted versus N_{part} which means that the enhancement of $\bar{p}$ over π^- is controlled by the initial size of created systems. Fig. 10 shows the comparison of BRAHMS and PHENIX data for the ratio of protons to positive pions measure at $y = 0$ with the theoretical calculation based on parton recombination [26] and on hydrodynamic [28] models. (more input will came from Eun-Joo)

5. HIGH p_T SUPPRESSION

Particles with high p_T (above 2 GeV/c) are primarily produced in hard scattering processes early in the collision. In high energy nucleon-nucleon reactions hard scattered partons fragment into jets of hadrons. However, in nucleus-nucleus collision hard scattered partons travel in the medium. If the medium is QGP the partons will lose a large fraction of their energy by induced gluon radiation, effectively leading to suppression of jet production [29]. Experimentally this phenomenon, known as a Jet Quenching, will be observed as a depletion of the high p_T region in hadron spectra.

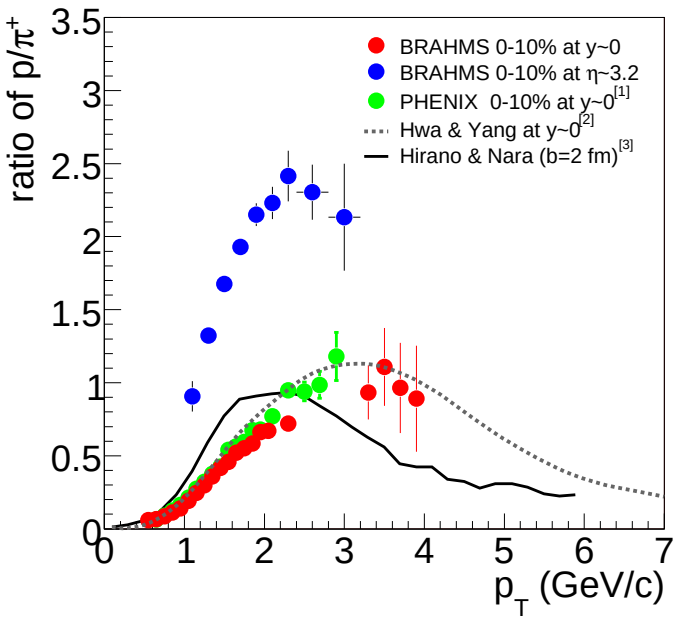

Figure 10. The p/π^+ versus p_T for Au + Au collisions at $\sqrt{s_{NN}}$ = 200 GeV measured at mid-rapidity by BRAHMS (circles) and by PHENIX (?? symbols).. The plotted lines show model calculations (see text).

The measure commonly used to study the medium effects is called the nuclear modification factor, R_{AA}. It is defined as a ratio of the particle yield produced in nucleus-nucleus collision, scaled with the number of binary collisions (N_{coll}), and the particle yield produced in elementary nucleon-nucleon collision:

$$R_{AA} = \frac{Yield(AA)}{N_{coll} \times Yield(NN)} \tag{5}$$

As mentioned above, at the high p_T the particle production is dominated by hard scatterings, so in the absence of nuclear effects (when the nucleus-nucleus collision reduces to the superposition of elementary collisions) we expect R_{AA} to be 1. At low p_T , where the production rate scales rather with N_{part}, R_{AA} should converge to N_{part}/N_{coll} which is roughly 1/3 for central Au + Au at RHIC energies. $R_{AuAu} < 1$ at high p_T 's will indicate the suppression which, as has been discussed, is the indication for the Jet Quenching. At SPS there is no suppression, in fact it is well known that there is enhancement for p_T > 2 GeV/c and this so called Cronin effect is attributed to initial multiple scattering of reacting partons.

Another variable used to quantify nuclear effects, but does not depend on the elementary reference spectra, is R_{CP} , define as a ratio of R_{AuAu} at central nucleus - nucleus collisions to R_{AuAu} at peripheral collisions. The idea of using R_{CP} based on the expectation that any nuclear modification in peripheral collisions in not significant. We will show that, in general, the last statement is not true for $R_{CP} = R_{AuAu}(0-10\%)/R_{AuAu}(40-60\%)$.

Figure 11. R_{AuAu} measured at $\eta \approx 2$ and $\eta \approx 1$ for Au + Au at $\sqrt{s_{NN}} = 200$ GeV (upper row) and at $\sqrt{s_{NN}} = 62.4$ GeV (bottom row), for different centrality classes indicated on the plot. (p + p reference is based on ISR collider data)

5.1. Collision centrality and energy evolution of R_{AuAu} for Au + Au and Cu + Cu

The large set of data collected during the RHIC runs 4 has allowed us to carry out the study of the R_{AuAu} evolution on collision centrality and collision energy for two collision systems namely Au + Au and Cu + Cu. Figure 11 R_{AuAu} measured at $\eta \approx 2$ and $\eta \approx 1$ for Au + Au at $\sqrt{s_{NN}} = 200$ GeV (upper row) and at $\sqrt{s_{NN}} = 62.4$ GeV (bottom row), for different centrality classes indicated on the plot (see also [30]). For the most central collision the R_{AuAu} shows suppression for both energy, however the suppression is significantly stronger for the system colliding with larger energy. It is seen a sooth increase of R_{AuAu} towards less central collision, for $\sqrt{s_{NN}} = 200$ GeV resulting in approximate scaling with N_{coll} above $p_T > 2$ GeV/c, for $40 - 50\%$ central collisions. For $\sqrt{s_{NN}} = 62.4$ GeV already for $20 - 40\%$ centrality class the Cronin peak in clearly visible and R_{AuAu} reaches value of about 1.5 in the p_T range between 2.0 and 3.0 GeV. The observed trends are qualitatively consistent with picture in which there are two opositively acting mechanisms that influence the nuclear modification in the medium and high p_T range, namely: the jet quenching that dominates at central collisions and and Cronin type enhancement (k_T broadening or/and quark recombination) that take over for the more peripheral collisions.

The next figure (Fig. 12), presents similar comparison as shown on Fig. 11 but this time we compare two different systems, namely, Au + Au and Cu + Cu colliding at the same energy ($\sqrt{s_{NN}} = 62.4$ GeV). For Cu + Cu at $\sqrt{s_{NN}} = 62.4$ GeV the same trend of increasing R_{AuAu} with decreasing of the level of collision centrality reveals from the data, however, the Cronin type enhancement is present already for the most central collisions.

Summarizing the whole set of observation we conclude that the level suppression of the inclusive hadron spectra produced in nucleus nucleus collisions at RHIC energies in the p_T range above 2 GeV increases with increasing collision energy, collision centrality and the size of the colliding nuclei. The dependency on the last two variables can be replaced by only one dependency on N_{part} .

PS comment: we haven't shown the direct argument for what is stated in the last sentence but plotting R_{AuAu} versus N_{part} for (Au+Au and CuCu at 62) maybe would

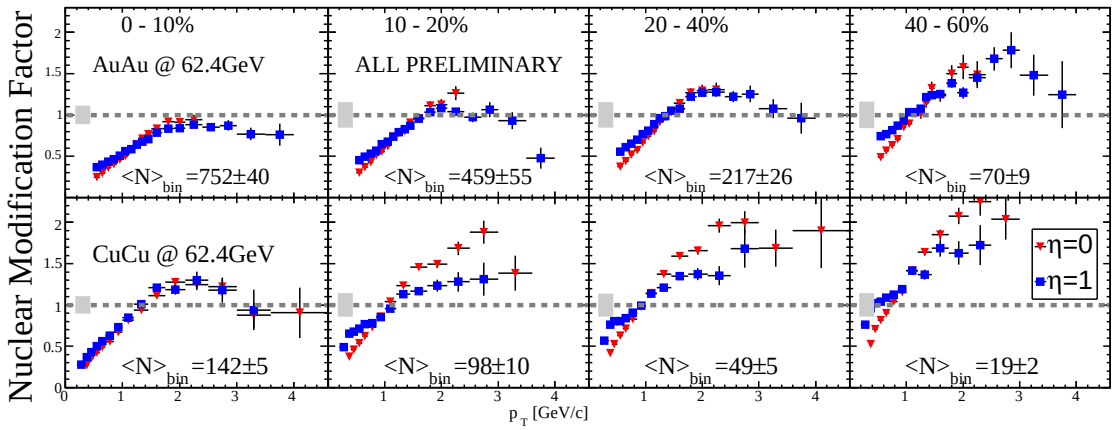

Figure 12. R_{AuAu} measured at mid-rapidity for Au + Au (upper row) and for Cu + Cu (bottom row) at $\sqrt{s_{NN}} = 62.4$ GeV for different centrality classes indicated on the plot. (p + p reference is based on ISR collider data)

show that? It looks like it can be done for eta=1.

5.2. R_{AuAu} for identified hadrons at forward rapidity for Au + Au at $\sqrt{s_{NN}} =$ 200 GeV

BRAHMS collaboration has already announced a large suppression of the nuclear modification factor (similar to that seen at mid rapidity) measured at large pseudo rapidity of $\eta = 2.2$ in Au + Au at $\sqrt{s_{NN}} = 200$ GeV [4]. However, the data did not allow to verify the mechanism responsible for the observed effect. In this section we present more exclusive analysis of nuclear effects at forward rapidity for identified pions, kaons and protons.

Figure 13 shows R_{AuAu} for identified hadrons at rapidity $y \approx 3.2$ for $0 - 10\%$ central Au+Au events at $\sqrt{s_{NN}} = 200$ GeV. The shaded band around unity indicates systematic error associated the with uncertainty in the number of binary collisions. Both R_{AuAu} and R_{CP} show suppression for pions (left panel) and for kaons (middle panel), however protons (right panel) R_{CP} shows suppression whereas R_{AuAu} reveals the Cronin type enhancement. with the peak at $p_T \approx 2$ GeV/c. The difference between R_{AuAu} and R_{CP} is striking, indicating significant enhancement of protons (in respect to p + p) for the $40 - 60\%$ collision centrality used in the definition of R_{CP} . The same misleading behavior of R_{CP} is seen for charge hadrons when comparing evolution of R_{CP} on η for Au + Au at $\sqrt{s_{NN}} = 200$ GeV and $\sqrt{s_{NN}} = 62.4$ GeV [30].

Figure 14 shows the nuclear modification factors calculated for $(\pi^+ + \pi^-)/2$ (left panel) and $(p + \bar{p})/2$ (right panel), respectively, at $y \approx 3.2$, for central Au + Au reaction. For the comparison we plotted the R_{AuAu} measured by the PHENIX Collaboration at mid rapidity. The R_{AuAu} measured for pions shows strong suppression (by factor of about 3 for $2 < p_T < 3$ GeV/c), both at mid and at forward rapidity. The consistency between mid and forward rapidity is seen also for protons, but in this case, R_{AuAu} reveals Cronin peak around $p_T = 2$ GeV/c. The similarity between R_{AuAu} at mid and forward rapidity observed simultaneously for pions and protons suggests same mechanisms responsible for the nuclear modifications within the studied rapidity interval.

It has been predicted [32] that the magnitude of quenching should depend on size

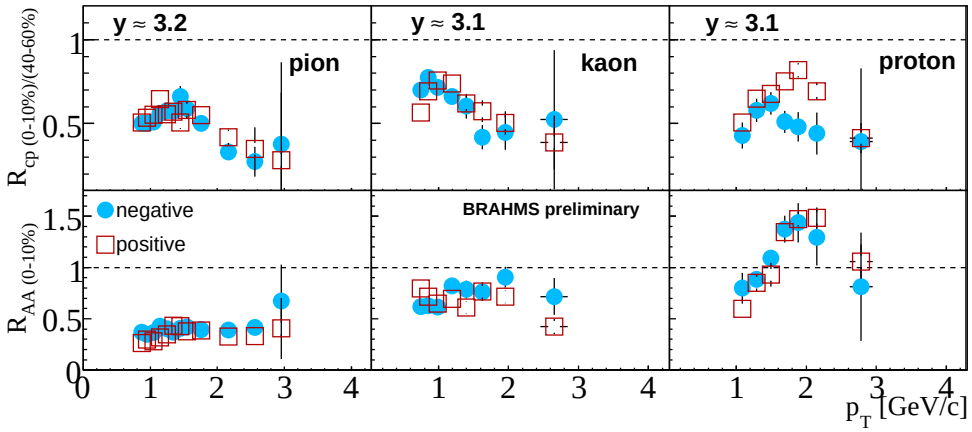

Figure 13. BRAHMS R_{AuAu} (upper row) and R_{CP} (bottom row) for pions, kaons and protons, measured $y \approx 3.2$ in Au + Au $\sqrt{s_{NN}} = 200$ GeV. The p + p reference was also measured by BRAHMS (see [31]).

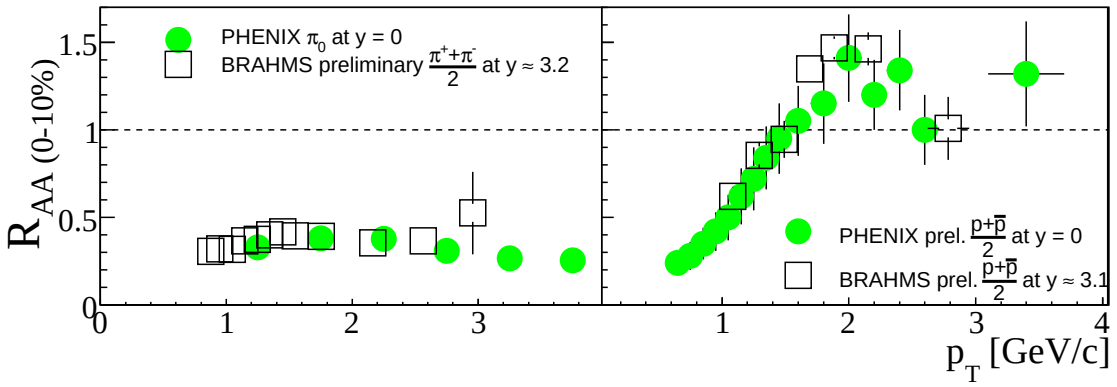

Figure 14. Comparison of R_{AuAu} measured for central Au + Au collisions at $\sqrt{s_{NN}} = 200$ GeV, at mid rapidity and $y = 3$ for pions (left panel) and protons (right panel).

and density of created absorbing medium, thus it is interesting to study the dependency of R_{AuAu} as the function of centrality. On Figure 15 we plotted the averaged R_{AuAu} measured for pions versus the N_{part} for mid rapidity (squared shape symbols) and for forward rapidity (triangles). The averaging was performed in the p_T range from 2 GeV/c to 3.5 GeV/c. It is seen again, that for the most central Au + Au reaction, the mid and forward pion suppression is of the same strength. However, the R_{AuAu} measure at forward rapidity shows significantly stronger rise towards peripheral collision as compare to R_{AuAu} at mid rapidity, that leads to the discrepancy on the level of 35% for $N_{part} = 100$. The trend is consistent with the model of parton energy loss in strongly absorbing medium [33,34]. In this picture, for $y = 0$, the jet emission is dominated by the emission for surface which quenches the dependency of R_{AuAu} on the system size. On the other hand, for $y \approx 3$, the transition from surface to volume emission can occur leading to stronger dependency on N_{part} .

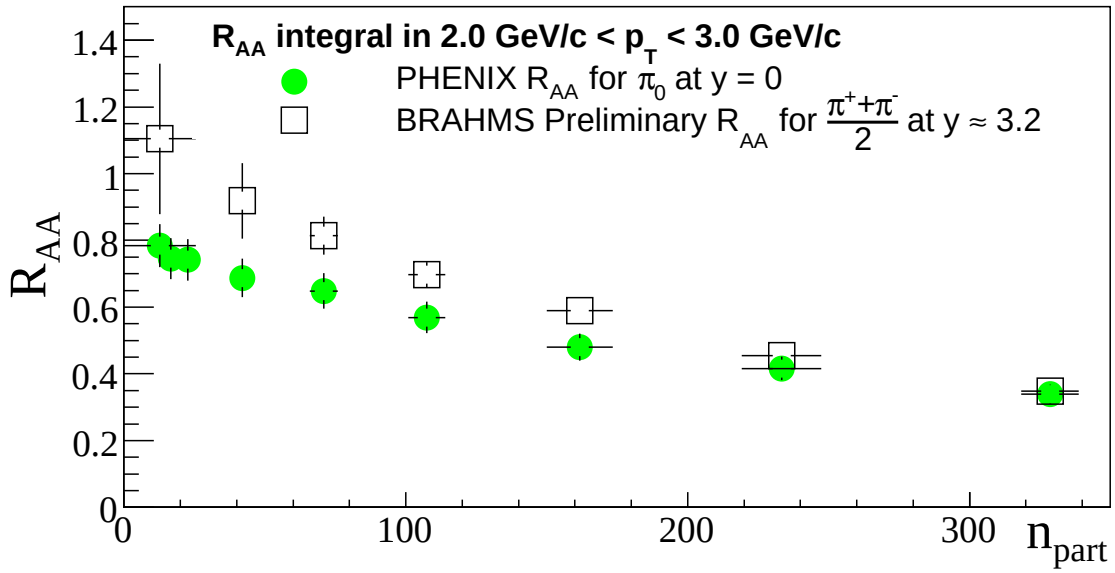

Figure 15. Average R_{AuAu} in the range $2.0 < p_T < 3.5$ GeV at mid rapidity (PHENIX) and at forward rapidity as a function of collision centrality, expressed by the number of participants.

6. SUMMARY

The results from BRAHMS and other RHIC experiments clearly show that studies of high energy nucleus - nucleus collisions have moved to a qualitatively new physics domain characterized by a high degree of reaction transparency leading to the formation of a near baryon free central region with approximate balance between matter and antimatter. The lower limit for the energy density at $\tau_o = 1$fm/c determined from the particle multiplicities and spectra is 5 GeV/fm^3 and 3.7 GeV/fm^3, for central Au + Au reactions at $\sqrt{s_{NN}} =$ 200 GeV and $\sqrt{s_{NN}} = 62.4$ GeV, respectively, therefore the conditions necessary for the formation of a deconfined system appear to be well fulfilled for the RHIC energies. Analysis within the statistical model of the relative abundances of π^-, π^+, p and $\bar{p}$ suggests the equilibrium at chemical freeze-out at temperature of 170 MeV with the noticeably strong correlation between strange and baryonic chemical potentials. The analysis of particle spectra within the blast-wave model suggests the kinetic freeze-out temperature of the order of 120 MeV and a large transverse expansion (with expansion velocity above 0.75c) which is consistent with the high initial energy density.

The measurement of the elliptic flow parameter v_2 versus rapidity and p_T shows weak dependency (if any) of the $v_2(p_T)$ on rapidity. The p/π rations measure within $0 < \eta < 3$ for Au + Au and Cu + Cu at $\sqrt{s_{NN}} = 62.4$ GeV and $\sqrt{s_{NN}} = 200$ GeV reveal strong enhancement of protons and anti-protons yields compared to pion yields. The observed enhancement is well understood within the quark coalescence/recombination models. We compare R_{AuAu} for Au + Au at $\sqrt{s_{NN}} = 200$ GeV and $\sqrt{s_{NN}} = 62.4$ GeV, and for Au + Au and Cu + Cu at $\sqrt{s_{NN}} = 200$ GeV. The general observed trend is that R_{AuAu} increases with: decreasing collision energy, system size, and collision centrality. For Au + Au central collisions at $\sqrt{s_{NN}} = 200$ GeV the R_{AuAu} shows very weak dependency on

rapidity (in $0 < y < 3.2$ interval), both for pions and protons.

REFERENCES

1. C. Adler *et al.* [STAR Collaboration], Phys. Rev. C**66** 034904 (2002). J. Adams *et al.* [STAR Collaboration], Phys. Rev. Lett. **92** 062301 (2004).
2. S. S. Adler *et al.* [PHENIX Collaboration], Phys. Rev. Lett. **91** 182301 (2003).
3. P. F. Kolb and U. Heinz, nuct-th/0305084, and references therein.
4. I. Arsene *et al.* [BRAHMS Collaboration], Phys. Rev. Lett. **91** (2003) 072305.
5. D. Kharzeev, Y. V. Kovchegov, and K. Tuchin Phys. Lett. B599 (2004) 23, and references therein.
6. C. Adler *et al.* [STAR Collaboration], Phys. Rev. Lett. **90** 082302 (2003).
7. C. Adler *et al.* [STAR Collaboration], Nucl. Phys. A **715** 272 (2003).
8. I. Arsene *et al.* [BRAHMS Collaboration], Phys. Rev. Lett. **93** 242303 (2004)
9. J. Jalilia-Marian, Nucl. Phys. A **748** 664 (2005).
10. M. Adamczyk *et al.* [BRAHMS Collaboration], Nucl. Instr. and Meth. A **499** (2003) 437.
11. D. Kharzeev and E. Levin, Phys. Lett. B **599** (2001) 79.
12. I. G. Bearden *et al.* [BRAHMS Collaboration], Phys. Lett. B523 (2001) 227.
13. I. G. Bearden *et al.* [BRAHMS Collaboration], Phys. Rev. Lett. **88** (2002) 202301.
14. G. J. Alner *et al.*, Z. Phys. C**33**, 1 (1986).
15. J. D. Bjorken, Phys. Rev. D **27** (1983) 140.
16. I. G. Bearden *et al.* [BRAHMS Collaboration], submitted to Phys. Ref. Lett. (nucl-ex/0403050)
17. F. Karsch, Nucl. Phys. A **698** (2002) 199.
18. I. G. Bearden *et al.* [BRAHMS Collaboration], Phys. Rev. Lett. **93** (2004) 102301.
19. I. G. Bearden *et al.* [BRAHMS Collaboration], Phys. Rev. Lett. **90** (2003) 102301.
20. F. Becattini *et al.*, Phys. Rev. C**64** 024901 (2001).
21. H. Ito [BRAHMS Collaboration], this volume.
22. C. E. Jørgensen *et al.* [BRAHMS Collaboration], Nucl. Phys. A **715** (2003) 741c.
23. Z. Yin *et al.* [BRAHMS Collaboration], J. Phys. G **30** (2004) S983.
24. R. J. Fries *et al.* Phys. Rev. C**68** 044902 (2003).
25. V. Greco, C. M. Ko, and I. Vitev, *et al.* Phys. Rev. C**71** 041901R (2005).
26. R. C. Hwa and C. B. Yang, Phys. Rev. C**70** (2004) 024905.
27. Eun Joo Kim [BRAHMS Collaboration], this volume.
28. T. Hirano, and Y. Nara Phys. Rev. C**68** (2003) 064902
29. Phys. Rev. C**58** 2321(1998).
30. T. M. Larsen [BRAHMS Collaboration], this volume.
31. R. Karabowicz [BRAHMS Collaboration], this volume.
32. M. Gyulassy, P. Levai, and I. Vitev, Nucl. Phys. B**594** (2001) 371. M. Gyulassy, P. Levai, and I. Vitev, Phys. Rev. D**66** (2002) 014005.
33. A. Dainese, C. Loizides, and G. Paić, Eur. Phys. J. C38 (2005) 461-474.
34. A. Drees, H. Feng, J. Jia, Phys. Rev. C**71** (2005) 034909.